Inorganic Chemistry
including bioinorganic chemistry

April 7, 2014
Volume 53, Number 7
pubs.acs.org/IC

Rational Loading of Luminescent Lanthanidopolymers

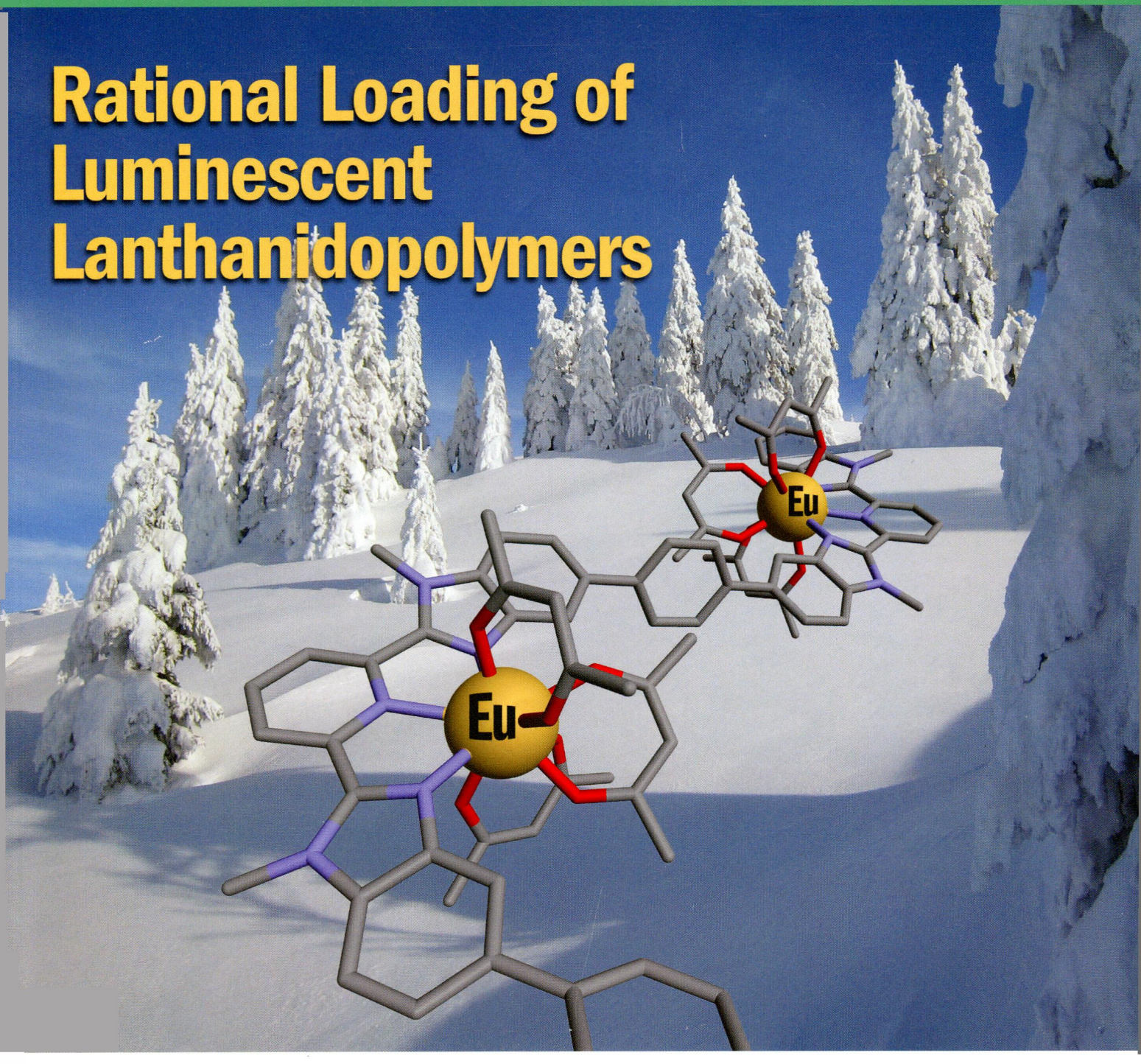

ACS Publications
MOST TRUSTED. MOST CITED. MOST READ.

www.acs.org

Inorganic Chemistry

APRIL 7, 2014
VOLUME 53 ISSUE 7

INOCAJ 53(7) 3257–3920 (2014)
ISSN 0020-1669
Registered in the U.S. Patent and Trademark Office

ON THE COVER: The combination of basic statistical mechanics with coordination chemistry allowed the controlled and rational loading of linear luminescent multisite polymers. See L. Babel, T. N. Y. Hoang, H. Nozary, J. Salamanca, L. Guénée, and C. Piguet, p 3568.

Communications

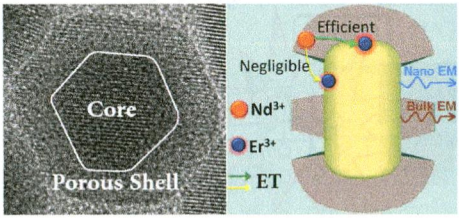

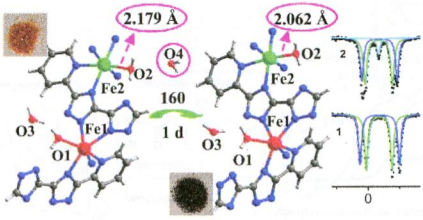

3263 S dx.doi.org/10.1021/ic500017a

Breakdown of the Energy Gap Law in Molecular Lanthanoid Luminescence: The Smallest Energy Gap Is Not Universally Relevant for Nonradiative Deactivation

Christine Doffek, Jessica Wahsner, Elisabeth Kreidt, and Michael Seitz*

This Communication shows experimentally that the energy gap law is not universally valid for the quantitative description of nonradiative deactivation in near-IR luminescent lanthanoid complexes featuring high-energy oscillators.

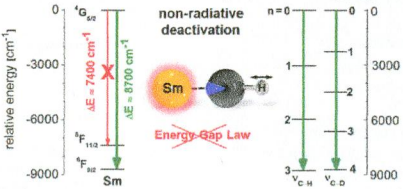

3266 S dx.doi.org/10.1021/ic500068x

New Nanostructured Zinc Phosphite Templated by Cetyltrimethylammonium Cations: Synthesis, Crystal Structure, Adsorption, and Photoluminescence Properties

Chih-Min Wang,* Tsung-Yuan Chang, Cheng-Wei Chiu, Hsiu-Mei Lin, and Kwang-Hwa Lii*

The first example of nanostructured zinc phosphite containing cetyltrimethylammonium (CTA^+) cations as a template, $(CTA)ZnBr(HPO_3)$, was synthesized using a hydro(solvo)thermal method and structurally characterized by single-crystal X-ray diffraction. Its 2D sheet structure consists of ZnO_3Br and HPO_3 units, which are sandwiched by CTA^+ ions with an interlayer d spacing of 28.05 Å. The adsorption and photoluminescence properties have also been studied.

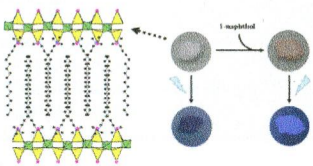

3269 S dx.doi.org/10.1021/ic500157x

Enantiomerically Pure Lanthanide–Organic Polytungstates Exhibiting Two-Photon Absorption Properties

Wei-Wei Ju, Hai-Tao Zhang, Xiao Xu, Yu Zhang, and Yan Xu*

Using the lanthanide tartrate coordination centers and lacunary Keggin polyoxometalate (POM) ions as achiral building blocks, two enantiomerically pure polytungstates, $Na_2[(CH_3)_2NH_2]_3\{NaC[Ce^{III}(H_2O)(CH_3CH_2OH)(L\text{-}tartH_3)(H_2Si_2W_{19}O_{66})]\}\cdot 3.5H_2O$ (L-**1**) and $[(CH_3)_2NH_2]_7\{NaC[Ce^{III}(H_2O)(CH_3CH_2OH)(D\text{-}tartH_3)(Si_2W_{19}O_{66})]\}\cdot 2.5H_2O$ (D-**1**), were successfully synthesized. Structural analysis indicates that the chiral organic ligands covalently bond to the lacunary polytungstate units. Significantly, these two new enantiomerically pure nanosized polytungstates are built from a novel polytungstate inorganic cluster, $[Si_2W_{19}O_{66}]^{10-}$, and cerium tartrate coordination centers with one sodium wrapped. Strong induced optical activity in the POM units is manifested by circular dichroism spectroscopy as a result of chirality transfer from an enantiopure organic molecule, that is, L- or D-tartaric acid, to inorganic clusters. Both enantiomeric complexes L-**1** and D-**1** show good third-order nonlinear optical responses.

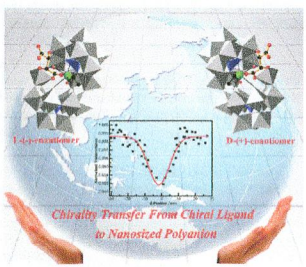

3272 dx.doi.org/10.1021/ic500299s

Ruthenium Tris(2-pyridylmethyl)amine as an Effective Photocaging Group for Nitriles

Rajgopal Sharma, Jessica D. Knoll, Philip D. Martin, Izabela Podgorski, Claudia Turro, and Jeremy J. Kodanko*

The photochemical release of nitriles from the caging fragment ruthenium tris(2-pyridylmethyl)amine (TPA) was studied. Caged complexes of the general formula $[Ru(TPA)(RCN)_2]^{2+}$ are stable in the dark but release a single nitrile upon irradiation with 365 nm light. Photoactivated inhibition of cathepsin K was demonstrated with a caged inhibitor complex.

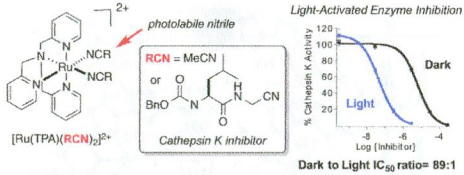

3275 dx.doi.org/10.1021/ic500326u

Luminescent Heteroleptic Tris(dipyrrinato)indium(III) Complexes

Shinpei Kusaka, Ryota Sakamoto,* and Hiroshi Nishihara*

To provide an improvement over the low fluorescence efficiencies often shown by homoleptic tris(dipyrrinato)indium(III) complexes, luminescent heteroleptic tris(dipyrrinato)indium(III) complexes bearing two types of dipyrrinato ligands are designed here by theoretical calculation and then synthesized. They possess frontier orbitals linked to suppression of the nonemissive charge-separated states; one shows a high fluorescence quantum yield (0.41) in toluene, which exceeds that of the corresponding BF_2 complex.

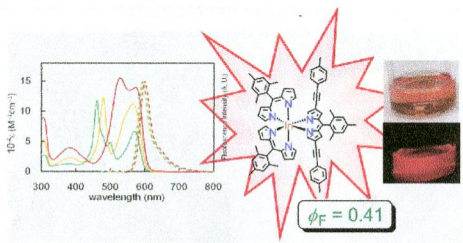

3278 dx.doi.org/10.1021/ic5003594

A 3-Fold-Symmetric Ligand Based on 2-Hydroxypyridine: Regulation of Ligand Binding by Hydrogen Bonding

Cameron M. Moore, David A. Quist, Jeff W. Kampf, and Nathaniel K. Szymczak*

A tripodal ligand based on 2-hydroxypyridine is presented. Cu−Cl adducts of H_3thpa with Cu^I and Cu^{II} provide complexes featuring highly directed, intramolecular hydrogen-bonding interactions. An upper limit for the hydrogen-bonding free energy to Cu^I−Cl was estimated at ~18 kcal/mol.

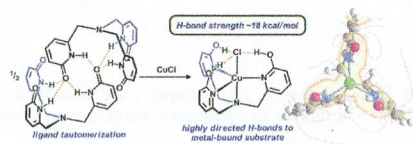

Articles

3307 S dx.doi.org/10.1021/ic402107z

Transition Metal Chlorides Are Lewis Acids toward Terminal Chloride Attached to Late Transition Metals

Alice K. Hui, Brian J. Cook, Daniel J. Mindiola, and Kenneth G. Caulton*

Reacting the different pincer ligands L with MCl_2 (M = Co or Cu) < 1:1 mol ratio leads to $(LMCl_2)_2{\cdot}MCl_2$, aggregated by MCl_2 linking together $LMCl_2$ units.

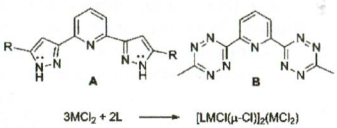

3311 S dx.doi.org/10.1021/ic402118u

Effect of Substituents on the Water Oxidation Activity of $[Ru^{II}(terpy)(phen)Cl]^+$ Procatalysts

Dakshika C. Wanniarachchi, Mary Jane Heeg, and Cláudio N. Verani*

The catalytic properties of a series of ruthenium procatalysts based on terpyridine and phenanthroline ligands toward water oxidation are evaluated, taking into account the effects of electron-donating and -withdrawing substituents. We observe that, despite structural similarities with well-known terpyridine/bipyridine systems, the opposite catalytic behavior is observed. Both the nature and position of the substituents on phenanthroline determine the optimized turnover numbers. Interestingly, the chloro procatalyst core is recovered after reaction.

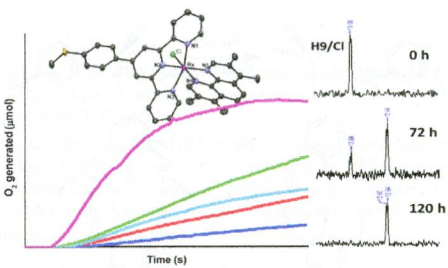

3320 S dx.doi.org/10.1021/ic402404a

A Nitrate Nonlinear Optical Crystal $Pb_{16}(OH)_{16}(NO_3)_{16}$ with a Large Second-Harmonic Generation Response

Lixian Chang, Li Wang,* Xin Su, Shilie Pan,* Reshalaiti Hailili, Hongwei Yu, and Zhihua Yang

A nitrate nonlinear optical crystal $Pb_{16}(OH)_{16}(NO_3)_{16}$ combines a planar triangle π-conjugated $[NO_3]^-$ system and PbO_n polyhedra with a large second-harmonic generation response that is 3.5 times as large as that of KH_2PO_4, and it is type I phase-matchable. More importantly, such second-harmonic generation behavior has not been reported previously for such a lead nitrate hydroxide compound.

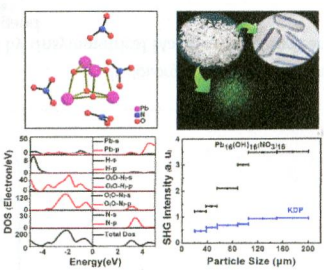

3326 S dx.doi.org/10.1021/ic500050q

Photocatalytic CO_2 Reduction in *N,N*-Dimethylacetamide/Water as an Alternative Solvent System

Yusuke Kuramochi, Masaya Kamiya, and Hitoshi Ishida*

N,N-Dimethylacetamide (DMA) has been used for the first time as the reaction solvent in the photocatalytic CO_2 reduction. The solvent is highly stable against hydrolysis and does not produce formate even if it is hydrolyzed. The photocatalytic system consisting of $[Ru(bpy)_2(CO)_2](PF_6)_2$ (bpy = 2,2′-bipyridine), $[Ru(bpy)_3](PF_6)_2$, and 1-benzyl-1,4-dihydronicotinamide (BNAH) efficiently reduces CO_2 to carbon monoxide (CO) and formate in DMA/water. In this work, the photoreaction is compared to the one in *N,N*-dimethylformamide (DMF)/water.

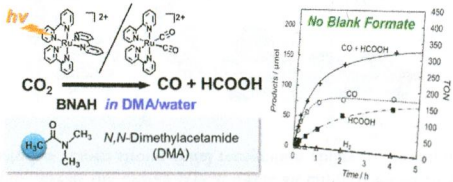

3333 S dx.doi.org/10.1021/ic402612v

Effect of Ligand Substituent Coordination on the Geometry and the Electronic Structure of Cu(II)-Diradical Complexes

Richa Rakshit, Samir Ghorai, Soumava Biswas, and Chandan Mukherjee*

The extent of interaction between the Cu(II) center and the donor atom that belongs to a substituent attached at the ortho position of the aniline moiety of 2-anilino-4,6-di-*tert*-butylphenol determines the geometry, ground state electronic configuration, and the energy differences between the electronic states in the corresponding Cu(II)-diradical complexes.

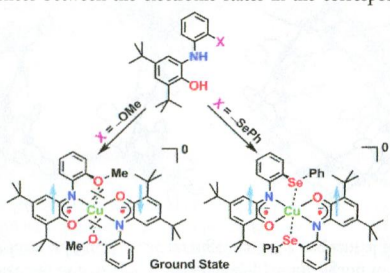

3338 S dx.doi.org/10.1021/ic402624u

Reversible Mechanochromic Luminescence at Room Temperature in Cationic Platinum(II) Terpyridyl Complexes

Ali Han, Pingwu Du,* Zijun Sun, Haotian Wu, Hongxing Jia, Rui Zhang, Zhenning Liang, Rui Cao,* and Richard Eisenberg*

A series of salts of the cationic chloroplatinum(II) terpyridyl complex have been synthesized and characterized. The salt containing the triflate anion shows an interesting reversible mechanochromic response at room temperature. A combination of spectroscopic methods, X-ray crystallographic analyses, and luminescent decay measurements lead to the conclusion that the mechanochromic response occurs as a result of a change in intermolecular Pt···Pt distances upon grinding.

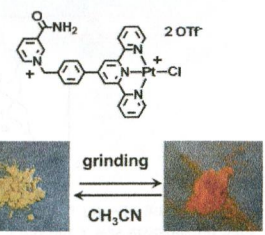

3345 dx.doi.org/10.1021/ic500193n

Fluoride Ion Sensing and Caging by a Preformed Molecular D4R Zinc Phosphate Heterocubane

Alok Ch. Kalita and Ramaswamy Murugavel*

Zinc phosphates featuring a D4R cage as the central core capture fluoride ions in solution preferentially over other ions. The present work demonstrates for the first time how a preformed molecular cage can selectively act as a host for fluoride ions. NMR studies and X-ray diffraction reveal the integrity of the D4R core during the process of fluoride uptake.

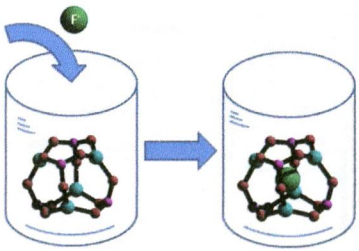

3354 dx.doi.org/10.1021/ic402717x

Mechanismic Investigation on the Cleavage of Phosphate Monoester Catalyzed by Unsymmetrical Macrocyclic Dinuclear Complexes: The Selection of Metal Centers and the Intrinsic Flexibility of the Ligand

Xuepeng Zhang, Yajie Zhu, Xiaowei Zheng, David Lee Phillips, and Cunyuan Zhao*

Herein, we report a theoretical work of the mechanismic investigation on the cleavage of phosphate monoester catalyzed by unsymmetrical macrocyclic dinuclear complexes. Five reaction mechanisms are proposed in consideration of the election of metal centers (zinc(II) or magnesium(II)), the intrinsic flexibility of the ligand (aromatic or not), and a functional second coordination sphere (hydrogen bonds between the catalyst and the substrate).

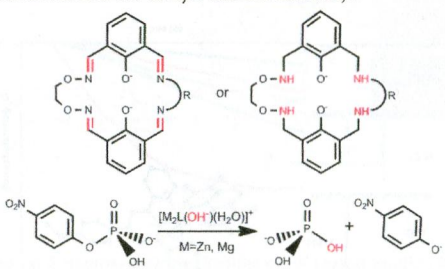

3362 S dx.doi.org/10.1021/ic402718c

3-D Silver(I)—Lanthanide(III) Heterometallic-Organic Frameworks Constructed from 2,2′-Bipyridine-3,3′-dicarboxylic Acid: Synthesis, Structure, Photoluminescence, and Their Remarkable Thermostability

Yunshan Zhou,* Xiaomin Li, Lijuan Zhang,* Yan Guo, and Zonghai Shi

The reactions between lanthanide oxides, the 2,2′-bipyridine-3,3′-dicarboxylic acid (H_2bpdc) ligand, and $AgNO_3$ under hydrothermal conditions resulted in the formation of eight remarkably thermostable 3-D (2,4,6)-connected silver-(I)—lanthanide(III) heterometallic-organic open frameworks of the fomula of $[AgLn(bpdc)_2]$ with $(4^{11}\cdot6^4)(4^3\cdot8^2\cdot10)(8)_2$ topology. The photoluminescence properties, energy transfer within the compounds, emission lifetimes, and the overall quantum yields were addressed.

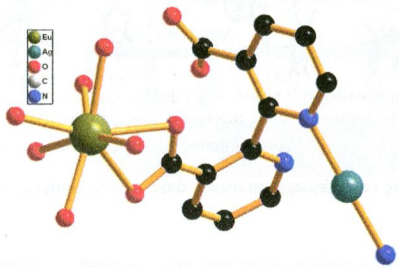

3371 S dx.doi.org/10.1021/ic402737f

Bispidine Analogues of Cisplatin, Carboplatin, and Oxaliplatin. Synthesis, Structures, and Cytotoxicity

Huiling Cui, Richard Goddard, Klaus-Richard Pörschke,* Alexandra Hamacher, and Matthias U. Kassack

Bispidine analogues **1**—**3** of cisplatin, carboplatin, and oxaliplatin have been prepared, including some DMF and water solute complexes. The crystal structures reveal various patterns of N—H···Cl and N—H···O hydrogen bonds. For the hydrates of **1** and **2**, different modes of water solvation were found. The compounds have been tested for their cytotoxicity against standard human cancer cell lines, revealing significant cytotoxic activity along with a low platinum resistance factor *R*.

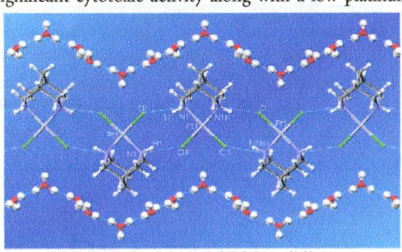

3385 S dx.doi.org/10.1021/ic4027915

Tetranuclear Lanthanide(III) Complexes in a Seesaw Geometry: Synthesis, Structure, and Magnetism

Joydeb Goura, James P. S. Walsh, Floriana Tuna,* and Vadapalli Chandrasekhar*

The reaction of the compartmental hydrazone ligand 2-methoxy-6-(pyridine-2-ylhydrazonomethyl)phenol (LH) with lanthanide (III) salts (Dy, Tb, Gd, and Ho) in the presence of an excess of triethylamine afforded a series of tetranuclear complexes in a highly unusual *seesaw* geometry. Magnetic studies allow the quantification of weak antiferromagnetic interactions in the Gd_4 complex, with the Dy_4 analogue exhibiting slow magnetic relaxation at low temperatures.

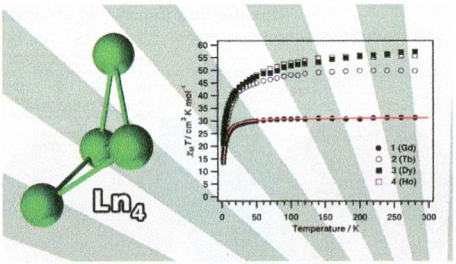

3392 S dx.doi.org/10.1021/ic402798f

Slow and Fast Singlet Energy Transfers in BODIPY-gallium(III)corrole Dyads Linked by Flexible Chains

Bertrand Brizet, Nicolas Desbois, Antoine Bonnot, Adam Langlois, Adrien Dubois, Jean-Michel Barbe, Claude P. Gros,* Christine Goze,* Franck Denat, and Pierre D. Harvey*

The direction of the singlet energy transfer in gallium(III)corrole-containing dyads can easily be reversed by putting no (BODIPY*→gallium(III)corrole), one (both directions), or two styryl groups (gallium(III)corrole*→BODIPY) on BODIPY. The rates of energy transfer in the latter case are 1 order of magnitude larger than the former. On the basis of the Förster resonance energy transfer theory (FRET), the dominant parameter explaining this difference is the J-integral (spectral overlap of the donor fluorescence with the acceptor absorption).

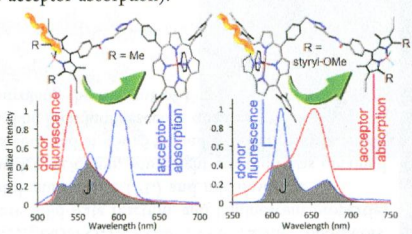

3404 S dx.doi.org/10.1021/ic402810e

Metal Ion Complexes of *N,N′*-Bis(2-Pyridylmethyl)-1,3-Diaminopropane-*N,N′*-Diacetic Acid, H_2bppd

Daniel S. Kissel, Jan Florián, Craig C. McLauchlan, and Albert W. Herlinger*

Complexation of trivalent metal ions (Al(III), Ga(III), In(III), and Co(III)) and selected lanthanides (Ln(III)) by *N,N′*-bis(2-pyridylmethyl)-diaminopropane-*N,N′*-diacetic acid (H_2bppd) was investigated. The X-ray structure for [Ga(bppd)]PF_6 shows the Ga atom residing in a distorted octahedral coordination environment with *cis*-acetate and *cis*-2-pyridylmethyl groups, in contrast to other [M(bppd)]$^+$ complexes that show *trans*-acetate coordination. IR, ^{1}H, and ^{13}C NMR spectroscopies and quantum mechanical calculations were used to differentiate among different types carboxylate bonding modes and cis and trans geometric isomers of pseudo-octahedral [M(bppd)]$^+$ complexes.

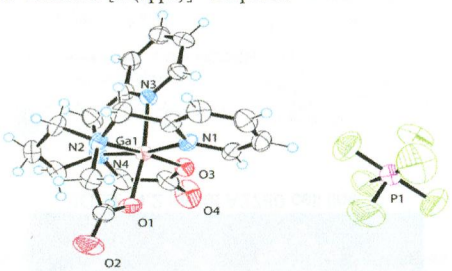

3417 S dx.doi.org/10.1021/ic402827b

Hydroxide-Free Cubane-Shaped Tetranuclear [Ln_4] Complexes

Sourav Das, Atanu Dey, Sourav Biswas, Enrique Colacio,* and Vadapalli Chandrasekhar*

We report the synthesis, structure, and magnetic properties of three tetranuclear lanthanide complexes having a distorted cubane-like core. The magnetic properties of the Dy(III) analogue show two-step relaxation with the following anisotropic barriers and pre-exponential factors: Δ/k_B = 73(2) K, $\tau_0 = 4.4 \times 10^{-8}$ s (slow relaxation); Δ/k_B = 47.2(9) K, $\tau_0 = 5.0 \times 10^{-7}$ s (fast relaxation).

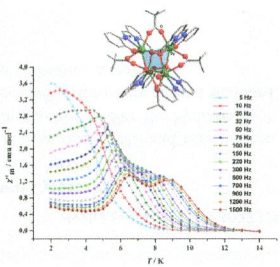

3427 S dx.doi.org/10.1021/ic402837n

Qualitative Estimation of the Single-Electron Transfer Step Energetics Mediated by Samarium(II) Complexes: A "SOMO–LUMO Gap" Approach

Christos E. Kefalidis,* Stéphanie Essafi, Lionel Perrin,* and Laurent Maron*

The inspection of the nature of the SOMO and LUMO in divalent lanthanide-substrate adducts is diagnostic of a potential single-electron transfer (SET) process. The SOMO–LUMO gap gives a qualitative indication of the SET.

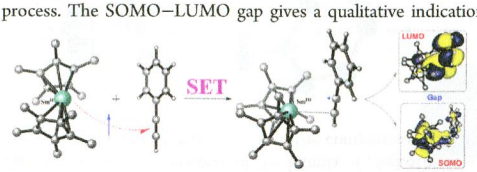

3434 dx.doi.org/10.1021/ic402867x

Obtaining Chiral Metal–Organic Frameworks via a Prochirality Synthetic Strategy with Achiral Ligands Step-by-Step

Huan Dong, Hailiang Hu, Yang Liu, Jun Zhong, Guangju Zhang, Fangfang Zhao, Xuhui Sun, Youyong Li, and Zhenhui Kang*

Construction of chiral frameworks via prochirality synthetic strategy with achiral ligands step-by-step.

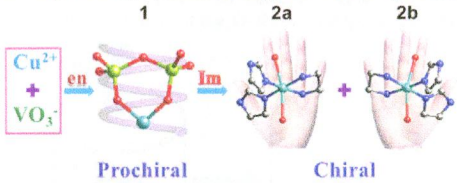

3441 dx.doi.org/10.1021/ic402870p

A Highly Efficient White Light $(Sr_3,Ca,Ba)(PO_4)_3Cl:Eu^{2+}$, Tb^{3+}, Mn^{2+} Phosphor via Dual Energy Transfers for White Light-Emitting Diodes

Xi Chen, Pengpeng Dai,* Xintong Zhang,* Cong Li, Shan Lu, Xiuli Wang, Yan Jia, and Yichun Liu

A series of single-phased $(Sr_{3-x,y}Ca_{1-y-z},Ba)(PO_4)_3Cl:xEu^{2+}$, yTb^{3+}, zMn^{2+} phosphors were synthesized by high-temperature solid-state reaction, and luminescent properties were investigated by means of photoluminescence (PL) and microcathode luminescence (μ-CL). Under ultraviolet excitation, white-light emission was obtained via combining three emission bands centered at 450, 543, and 570 nm contributed by Eu^{2+}, Tb^{3+}, and Mn^{2+}, respectively. The high luminescence quantum yield (51.2–81.4%) can be tuned by controlling the content of Eu^{2+}, Tb^{3+}, and Mn^{2+}.

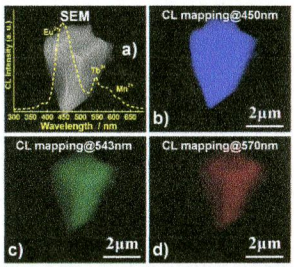

3449 dx.doi.org/10.1021/ic402886t

Alignment of Palladium Complexes into Columnar Liquid Crystals Driven by Peripheral Triphenylene Substituents

Emiliano Tritto, Rubén Chico, Gerardo Sanz-Enguita, César L. Folcia, Josu Ortega, Silverio Coco, and Pablo Espinet*

Mono- and dinuclear ortho-palladated complexes based on a triphenylene-imine ligand that display columnar mesophases (Col) at temperatures close to ambient have been isolated. The mesophase stability is large, and their structures consist of Pd-containing columnar zones supported by fully organic columns formed by the triphenylene moieties.

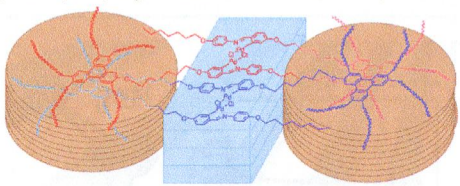

3456 S dx.doi.org/10.1021/ic402900x

Imparting Tunable and White-Light Luminescence to a Nanosized Metal–Organic Framework by Controlled Encapsulation of Lanthanide Cations

You Zhou and Bing Yan*

Nanocrystals of MOF **1** were fabricated in a capping agent- and surfactant-free solvothermal system. Subsequently, Ln^{3+} cations were incorporated into the pores of these nanocrystals for generating a new class of MOFs with tunable and white-light luminescence.

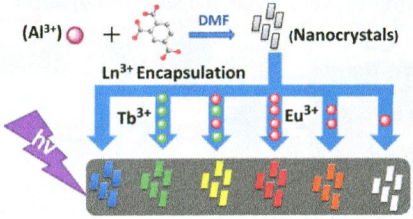

3464 S dx.doi.org/10.1021/ic402910a

Copper-Organic/Octamolybdates: Structures, Bandgap Sizes, and Photocatalytic Activities

Lan Luo, Haisheng Lin, Le Li, Tatyana I. Smirnova, and Paul A. Maggard*

The synthesis and visible-light photocatalytic activity are described for $[Cu(pda)]_4[\beta\text{-}Mo_8O_{26}]$ (**I**), consisting of layers of copper(I)-tetramer/octamolybdate clusters, and for two related Cu(II)-containing octamolybdate structures. Only compound **I** exhibits visible-light photocatalytic activity for oxygen production, owing to a bandgap size of ~1.8 eV that arises from an electronic excitation between the Cu(I)-tetramer (yellow shading) and the octamolybdate cluster (blue shading).

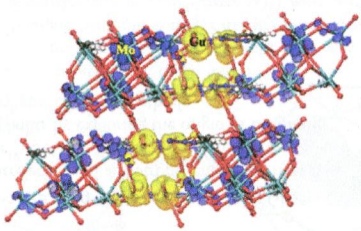

3471 dx.doi.org/10.1021/ic402913k

Structural and Relative Stabilities, Electronic Properties, and Hardness of Iron Tetraborides from First Prinicples

Li-Ping Ding, Xiao-Yu Kuang,* Peng Shao, and Xiao-Fen Huang

First-principles calculations were performed on FeB_4 with various different structures. On the basis of the analyses of elastic constants, formation enthalpies, as well as phonon dispersions, we found that 58-FeB_4 is the most energetically stable structure and the other four new phases (12-, 59-, 166- and RuB_4–FeB_4) are dynamically stable. Analysis of DOS demonstrates these compounds all exhibit metallic behavior. Additionally, their Vickers hardness calculations indicate that 59-FeB_4 is a superhard material, while the others are predicted to be potential hard materials.

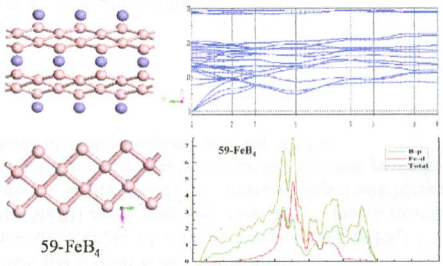

3480 dx.doi.org/10.1021/ic402926n

A New Type of Charge-Transfer Salts Based on Tetrathiafulvalene–Tetracarboxylate Coordination Polymers and Methyl Viologen

Yu-De Huang, Peng Huo, Ming-Yan Shao, Jing-Xue Yin, Wei-Chun Shen, Qin-Yu Zhu,* and Jie Dai*

A new type of charge-transfer salts {[cation]$^{n+}$·[TTFs]$^{n-}$} is designed in order to introduce a functional organic cation into the TTF–metal coordination polymer framework. The coordination center of the Mn(II) ion has a great effect on the enhancement of the photocurrent response.

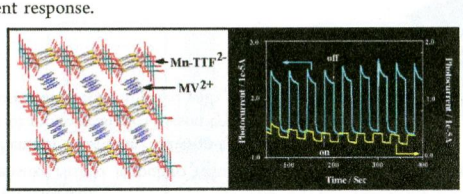

3488 dx.doi.org/10.1021/ic402932y

Promiscuous Ability of Human Carbonic Anhydrase: QM and QM/MM Investigation of Carbon Dioxide and Carbodiimide Hydration

Paolo Piazzetta, Tiziana Marino,* and Nino Russo

The high exothermicity of the carbodiimide hydration reaction is related to the stabilization of the product (ureate) in the active site. In the final product, the ureate moiety is coordinated to the Zn^{2+} prevalently by deprotonated nitrogen and is engaged in hydrogen bonds with the Thr199 and Thr200 residues.

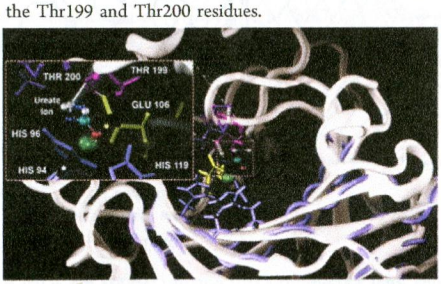

3494 Ⓢ dx.doi.org/10.1021/ic4029386

1D to 3D Heterobimetallic Complexes Tuned by Cyanide Precursors: Synthesis, Crystal Structures, and Magnetic Properties

Daopeng Zhang,* Weijiang Si, Ping Wang, Xia Chen, and Jianzhuang Jiang*

A series of five new cyanide-bridged heterobimetallic complexes structurally characterized as a one-dimensional cationic polymer and a two-dimensional and a three-dimensional network have been isolated by using a polyaza macrocycle nickel(II) compound and five cyanidometalate precursors containing different numbers of cyanide groups as building blocks. Their magnetic properties have been systematically and comparatively investigated.

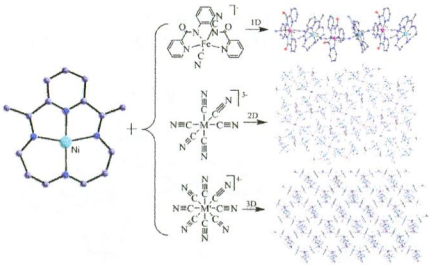

3503 dx.doi.org/10.1021/ic402945j

Magneto-Structural Correlations in a Family of $Fe^{II}Re^{IV}(CN)_2$ Single-Chain Magnets: Density Functional Theory and Ab Initio Calculations

Yi-Quan Zhang, Cheng-Lin Luo, Xin-Bao Wu, Bing-Wu Wang,* and Song Gao*

We obtained the expressions of the correlation and anisotropic energy barriers Δ_ξ and Δ_A with D, J, and S for six $Fe^{II}Re^{IV}(CN)_2$ SCMs in the intermediate region between the Ising and the Heisenberg limits by exploring the origin of the energy barriers using density functional theory and ab initio methods.

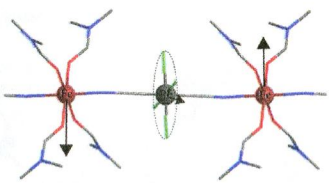

3511 Ⓢ dx.doi.org/10.1021/ic402948s

Reduced Graphene Oxide-Induced Recrystallization of NiS Nanorods to Nanosheets and the Improved Na-Storage Properties

Qin Pan, Jian Xie,* Tiejun Zhu, Gaoshao Cao, Xinbing Zhao,* and Shichao Zhang

Single-crystalline NiS nanorods are recrystallized into nanosheets induced by rGO. Chemical bonding occurs between surface dangling or unsaturated bonds on NiS rods and oxygen-containing groups on rGO sheets, that weakens the binding force between surface NiS layers and bulk NiS nanorods and results in the subsequent exfoliation of NiS layers. The NiS/G nanosheets exhibit better electrochemical Na-storage properties than NiS nanorods due to the unique sheetlike structure and the buffering and conducting effects of rGO.

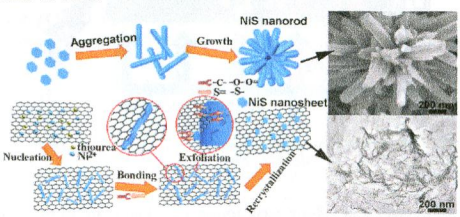

3519 S dx.doi.org/10.1021/ic402973g

Family of Defect-Dicubane Ni_4Ln_2 (Ln = Gd, Tb, Dy, Ho) and Ni_4Y_2 Complexes: Rare Tb(III) and Ho(III) Examples Showing SMM Behavior

Lang Zhao, Jianfeng Wu, Hongshan Ke, and Jinkui Tang*

A new family of defect-dicubane 3d–4f clusters were studied where slow relaxation of the magnetization under zero dc field was observed for the first time for the Ni–Tb and Ni–Ho systems.

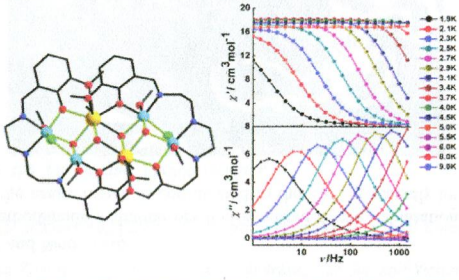

3526 S dx.doi.org/10.1021/ic403041s

Preparation and Redox Studies of α_1- and α_2-Isomers of Mono-Ru-Substituted Dawson-type Phosphotungstates with a DMSO Ligand: $[\alpha_1/\alpha_2\text{-}P_2W_{17}O_{61}Ru^{II}(DMSO)]^{8-}$

Shuhei Ogo, Noriko Shimizu, Kensuke Nishiki, Nobuhiro Yasuda, Tsutomu Mizuta, Tsuneji Sano, and Masahiro Sadakane*

Both α_1- and α_2-isomers of ruthenium substituted Dawson-type phosphotungstate were prepared from α_2-isomers of monolacunary Dawson-type phosphotungstate and Ru reagents. Their redox potentials were compared with the Keggin-derivatives.

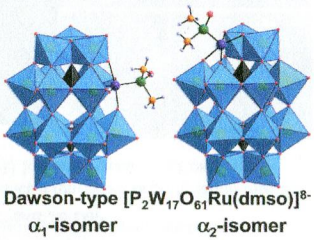

3540 S dx.doi.org/10.1021/ic403044x

$A_6U_3Sb_2P_8S_{32}$ (A = Rb, Cs): Quinary Uranium(IV) Thiophosphates Containing the $[Sb(PS_4)_3]^{6-}$ Anion

Jean-Marie Babo, Kariem Diefenbach, and Thomas E. Albrecht-Schmitt*

The quinary U(IV) thiophosphates $A_6U_3Sb_2P_8S_{32}$ (A = Rb, Cs) contain the $[Sb(PS_4)_3]^{6-}$ anion. This unit possesses a central Sb(III) cation bound by three $[PS_4]^{3-}$ anions, creating a trigonal pyramidal environment around Sb(III). The U(IV) centers are found with trimeric $[U_3S_{18}]^{24-}$ clusters. Magnetic susceptibility measurements indicate that the close proximity of the U(IV) within these clusters leads to antiferromagnetic ordering at 53 K.

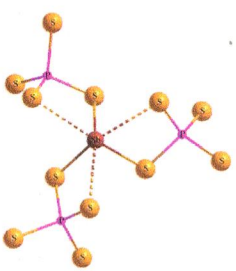

3546 dx.doi.org/10.1021/ic403035u

Polynuclear Iron(II)–Aminotriazole Spincrossover Complexes (Polymers) In Solution

Irene Bräunlich, Antoni Sánchez-Ferrer, Matthias Bauer, Rahel Schepper, Philippe Knüsel, Julia Dshemuchadse, Raffaele Mezzenga, and Walter Caseri*

Solutions of the spincrossover complex $[Fe(NH_2trz)_3](2ns)_2$ (NH_2trz = 4-amino-1,2,4-triazole, $2ns^-$ = 2-naphthalenesulfonate) in DMF were studied with UV/vis spectroscopy, X-ray absorption spectroscopy, and SAXS. Polynuclear species of different lengths were in equilibrium with each other. Linear rigid-rod $[Fe(NH_2trz)_3]^{2+}$ polymers (more than 100 Fe^{2+} ions) were established in the low-spin state in the presence of an excess of the ligand. An increase in temperature to 60 °C led to a reversible spin crossover.

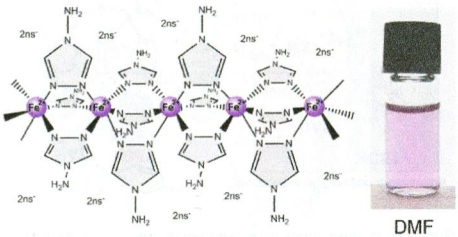

3558 dx.doi.org/10.1021/ic403050c

Tiara-like Octanuclear Palladium(II) and Platinum(II) Thiolates and Their Inclusion Complexes with Dihalo- or Iodoalkanes

Yukari Yamashina, Yasutaka Kataoka, and Yasuyuki Ura*

A tiara-like octanuclear palladium thiolate complex, $[Pd(\mu\text{-}SCH_2CO_2Me)_2]_8$, was synthesized via reactions of either $PdCl_2$ with methyl thioglycolate/*N*,*N*-diisopropylethylamine or $[PdCl_2(MeCN)_2]$ with *m*-$C_6H_4(CMe_2SCH_2CO_2Me)_2$. The latter method efficiently produced the corresponding platinum complex in high purity. Small molecules such as CH_2Cl_2 were accommodated in the inner voids. These complexes are stabilized by weak CH···X hydrogen bonds (X = Cl or Br) as well as weak coordination of the halogen atoms to the transition-metal atoms.

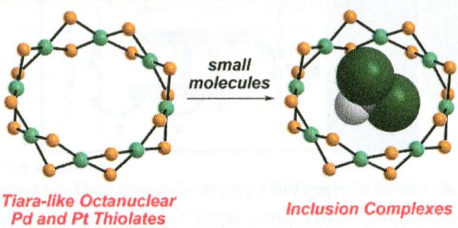

3568 dx.doi.org/10.1021/ic4030525

Lanthanide Loading of Luminescent Multi-Tridentate Polymers under Thermodynamic Control

Lucille Babel, Thi Nhu Y Hoang, Homayoun Nozary, Jasmina Salamanca, Laure Guénée, and Claude Piguet*

Using $[Ln(hfac)_3]$ as lanthanide carriers, the thermodynamic loading of linear multitridentate oligomers (green arrow) follows an anticooperative protocol compatible with the rational preparation of organized and luminescent (Ln = Eu) homo- and heterometallic Wolf type-II lanthanidopolymers.

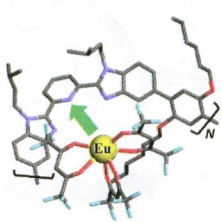

3579 S dx.doi.org/10.1021/ic4030684

Minimizing the Risk of Reporting False Aromaticity and Antiaromaticity in Inorganic Heterocycles Following Magnetic Criteria

Juan J. Torres-Vega, Alejandro Vásquez-Espinal, Julio Caballero, María L. Valenzuela, Luis Alvarez-Thon, Edison Osorio, and William Tiznado*

Searching for an adequate and simple test of aromaticity in inorganic heterocycles is of crucial interest due to the increasing research in the synthesis and evaluation of new inorganic rings conformed by the principal group elements. The aromaticity concept has been adopted and plays an important role in the emerging chemistry of these new compounds.

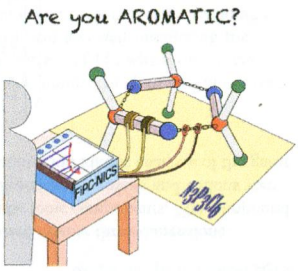

3586 S dx.doi.org/10.1021/ic403097s

Closely-Related $Zn^{II}_2Ln^{III}_2$ Complexes (Ln^{III} = Gd, Yb) with Either Magnetic Refrigerant or Luminescent Single-Molecule Magnet Properties

José Ruiz, Giulia Lorusso, Marco Evangelisti,* Euan K. Brechin,* Simon J. A. Pope, and Enrique Colacio*

Two tetranuclear complexes $\{(\mu_3\text{-}CO_3)_2[Zn(\mu\text{-}L)Gd(NO_3)]_2\}\cdot 4CH_3OH$ and $\{(\mu_3\text{-}CO_3)_2[Zn(\mu\text{-}L)Gd(NO_3)]_2\}\cdot 4CH_3OH$, with diphenoxo-bridging groups connecting Zn^{II} and Ln^{III} ions inside the ZnLn units and carbonato bridging anions connecting these dinuclear units, and one diphenoxo-bridged dinuclear complex $[Zn(\mu\text{-}L)(\mu\text{-}NO_3)Yb(NO_3)_2]$ ($H_2L = N_3O_4$ compartmental ligand) have been structurally and magnetically characterized. The Zn_2Dy_2 exhibits a large magneto-caloric effect, whereas the Yb^{III} complexes are bifunctional materials combining field-induced SMM behavior and well-resolved luminescence in the NIR region.

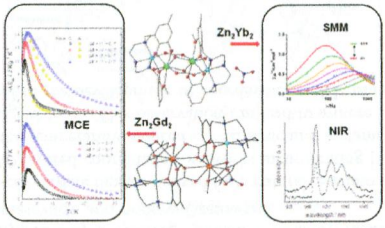

3595 S dx.doi.org/10.1021/ic403089j

Five-Coordinate $[Pt^{II}(bipyridine)_2(phosphine)]^{n+}$ Complexes: Long-Lived Intermediates in Ligand Substitution Reactions of $[Pt(bipyridine)_2]^{2+}$ with Phosphine Ligands

Warrick K. C. Lo, Germán Cavigliasso, Robert Stranger, James D. Crowley,* and Allan G. Blackman*

The isolation and X-ray structural characterization of $[Pt(bpy)_2\{PPh(PhSO_3)_2\}]\cdot 5.5H_2O$ provides evidence for the formation of 5-coordinate species from the reaction of $[Pt(N{-}N)_2]^{2+}$ (N−N = bpy, 4,4′-Me_2bpy) complexes with monodentate phosphine ligands in both aqueous and methanolic solution.

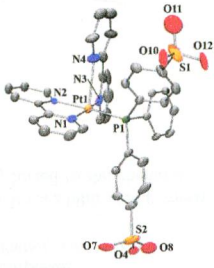

3606 S dx.doi.org/10.1021/ic403100h

Structure and Thermodynamic Properties of $(C_5H_{12}N)CuBr_3$: A New Weakly Coupled Antiferromagnetic Spin-1/2 Chain Complex Lying in the 1D−3D Dimensional Cross-Over Regime

Bingying Pan, Yang Wang, Lijuan Zhang,* and Shiyan Li*

A new weakly coupled Heisenberg antiferromagnetic spin-1/2 chain complex $(C_5H_{12}N)CuBr_3$ is reported. The chain structure is formed by edge-sharing $CuBr_5$ units. The magnetic susceptibility manifests typical HAFM spin chain behavior. The specific heat reveals two successive phase transitions in magnetic field. The static magnetic moment in the ordered state is $m_0 = 0.23\ \mu B$, making $(C_5H_{12}N)CuBr_3$ very suitable to study the dimensional cross-over problem in magnetism.

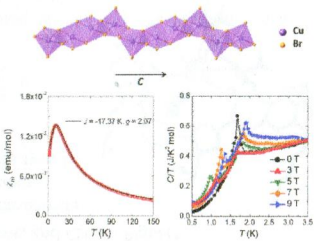

3611 S dx.doi.org/10.1021/ic403107v

Effect of Metal Coordination on Photocurrent Response Properties of a Tetrathiafulvalene Organogel Film

Shu-Fang Ji, Yong-Gang Sun, Peng Huo, Wei-Chun Shen, Yu-De Huang, Qin-Yu Zhu,* and Jie Dai*

The TTF-derived gels can coordinate to square coordination Ni(II) and Cu(II) ions, and the effect of the coordination on the photocurrent response properties is examined.

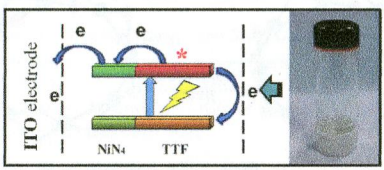

3618 S dx.doi.org/10.1021/ic403124u

Unified View of Oxidative C−H Bond Cleavage and Sulfoxidation by a Nonheme Iron(IV)−Oxo Complex via Lewis Acid-Promoted Electron Transfer

Jiyun Park, Yuma Morimoto, Yong-Min Lee, Wonwoo Nam,* and Shunichi Fukuzumi*

The mechanisms of both the oxidative C−H bond cleavage of toluene derivatives and sulfoxidation of thioanisole derivatives by $[(N4Py)Fe^{IV}(O)]^{2+}$ in the presence of HOTf and $Sc(OTf)_3$ have been unified as the rate-determining electron transfer, which is coupled with binding of $[(N4Py)Fe^{IV}(O)]^{2+}$ by proton (PCET) and $Sc(OTf)_3$ (MCET). The PCET and MCET reactivities of $[(N4Py)Fe^{IV}(O)]^{2+}$ with various Lewis acids have also been unified as a single correlation with a quantitative measure of the Lewis acidity.

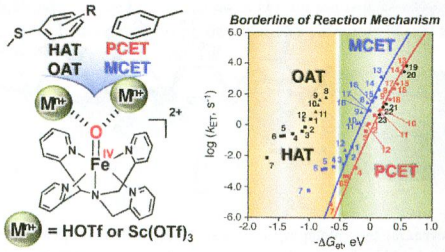

3629 dx.doi.org/10.1021/ic403138a

Photophysical and Photochemical Trends in Tricarbonyl Rhenium(I) N-Heterocyclic Carbene Complexes

Jamila G. Vaughan, Brodie L. Reid, Phillip J. Wright, Sushil Ramchandani, Brian W. Skelton, Paolo Raiteri, Sara Muzzioli, David H. Brown, Stefano Stagni,* and Massimiliano Massi*

The photochemistry of Re(I) complexes bound to bidentate N-heterocyclic carbene ligands proceeds via a bifurcated pathway involving direct CO dissociation and halogen exchange, with the photoreactivity being intimately linked to the chemical identity of the chelating ligand.

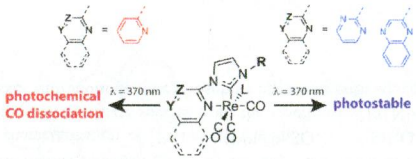

3642 dx.doi.org/10.1021/ic403148f

1,2,4-Triazolyl-Carboxylate-Based MOFs Incorporating Triangular Cu(II)-Hydroxo Clusters: Topological Metamorphosis and Magnetism

Sergiy I. Vasylevs'kyy, Ganna A. Senchyk, Andrey B. Lysenko,* Eduard B. Rusanov, Alexander N. Chernega, Julia Jezierska, Harald Krautscheid, Konstantin V. Domasevitch, and Andrew Ozarowski*

The heterobifunctional 1,2,4-triazolyl-carboxylate ligands derived from natural α-amino acids offer remarkable potential in the construction of 3D zeolite-like and 2D layered coordination networks incorporating [$Cu_3(\mu_3$-OH)] triangular clusters. The metal–organic frameworks undergo the temperature-induced crystal structural metamorphosis that displays intimate relationships between different topological types. This observation can lead to a more comprehensive understanding of such phenomena, reaction mechanisms, and to the development of coordination solids using solid-state reactions.

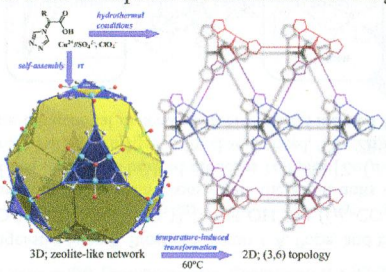

3655 dx.doi.org/10.1021/ic4031574

Concerted Functions of Anions and Cations in a Molecular Ionic Crystal with Stable Three-Dimensional Micropores

Ryosuke Kawahara, Sayaka Uchida,* and Noritaka Mizuno*

A molecular ionic crystal [$Cr_3O(OOCCH{=}CH_2)_6(H_2O)_3]_3[\alpha$-$PW_{12}O_{40}$] was synthesized. Stable three-dimensional micropores were constructed for the first time with discrete and precisely located molecular ionic components. The compound showed shape-selective sorption of CO_2 and C_2H_2 over N_2 and methane. Concerted functions of anions and cations were suggested by detailed investigation of the crystal structure as well as Monte Carlo simulations and kinetic analyses of the guest sorption.

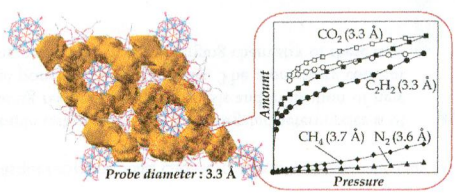

3662 S dx.doi.org/10.1021/ic403169z

Novel, Mercury-Free Synthetic Pathway for Trifluoromethylthio-Substituted Metallocenes

Jeannine Hess, Sandro Konatschnig, Sandra Morard, Vanessa Pierroz, Stefano Ferrari, Bernhard Spingler, and Gilles Gasser*

Trifluoromethylthioferrocene and its higher homologue trifluoromethylthioruthenocene, which is reported for the first time, were prepared in a reaction sequence involving first the treatment of the respective halogeno-metallocenes with NaSCN in the presence of copper(+I) to yield the thiocyanato-metallocenes and then the reaction of the latter with the Rupper-Prakash reagent and tetrabutylammonium fluoride to give the expected organometallic compounds in good yields. Importantly, this synthetic procedure does not involve the use of mercury reagents.

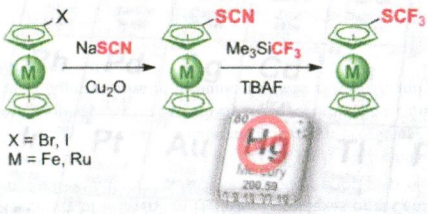

3668 S dx.doi.org/10.1021/ic403170y

Synthesis, Characterization, and Antitumor Activity of Water-Soluble (Arene)ruthenium(II) Derivatives of 1,3-Dimethyl-4-acylpyrazolon-5-ato Ligands. First Example of Ru(arene)(ligand) Antitumor Species Involving Simultaneous Ru–N7(guanine) Bonding and Ligand Intercalation to DNA

Francesco Caruso,* Elena Monti, Julian Matthews, Miriam Rossi, Marzia Bruna Gariboldi, Claudio Pettinari, Riccardo Pettinari, and Fabio Marchetti*

When the HQ^R ligands coordinate to Ru(arene)Cl, only the naphthyl moiety intercalates in DNA. The naphthyl is located below the guanine base establishing a $\pi-\pi$ interaction though a vertical line; meanwhile, Ru is bound to the corresponding N7(guanine). The Ru coordination sphere is ball style, and the remaining atoms in the Ru complex are stick style. DNA atoms are line style and aromatic (DNA, naphthyl, and cymene) centroids are green ball.

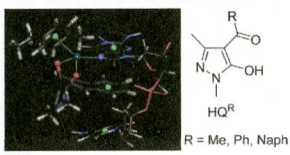

3678 S dx.doi.org/10.1021/ic403178j

The Stannylphosphide Anion Reagent Sodium Bis(triphenylstannyl) Phosphide: Synthesis, Structural Characterization, and Reactions with Indium, Tin, and Gold Electrophiles

Christopher C. Cummins,* Chao Huang, Tabitha J. Miller, Markus W. Reintinger, Julia M. Stauber, Isabelle Tannou, Daniel Tofan, Abouzar Toubaei, Alexandra Velian, and Gang Wu*

The sodium monophosphide $[Na][P(SnPh_3)_2]$, obtained by direct treatment of white phosphorus (P_4) with in situ generated $[Na][SnPh_3]$, is a competent precursor to the homoleptic phosphine $P(SnPh_3)_3$, the indium phosphide $(XL)_2InP(SnPh_3)_2$ ($XL = S(CH_2)_2NMe_2$), and the gold phosphide $(Ph_3P)AuP(SnPh_3)_2$ by reaction with an appropriate salt metathesis partner: $ClSnPh_3$, $(XL)_2InI$, or $(Ph_3P)AuCl$.

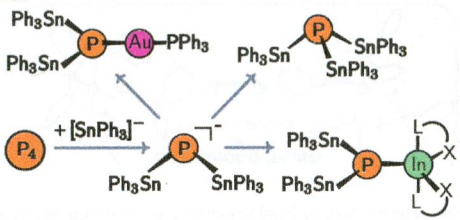

3688 S dx.doi.org/10.1021/ic500013c

A Confirmation of the Quench-Cryoannealing Relaxation Protocol for Identifying Reduction States of Freeze-Trapped Nitrogenase Intermediates

Dmitriy Lukoyanov, Zhi-Yong Yang, Simon Duval, Karamatullah Danyal, Dennis R. Dean, Lance C. Seefeldt, and Brian M. Hoffman*

We have advanced a mechanism for nitrogenase catalysis that rests on a quench-cryoannealing protocol for determining the number of electrons accumulated in an EPR-active freeze-trapped intermediate. The protocol involved monitoring the intermediate in frozen solution and following its relaxation to resting state through the release of H_2, which carries two reducing equivalents. This protocol implicitly predicts that states having accumulated an odd number of electrons cannot relax to resting. The present experiments confirm this prediction.

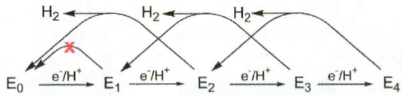

3694 S dx.doi.org/10.1021/ic5000205

Photosolvolysis of *cis*-[Ru(α-diimine)$_2$(4-aminopyridine)$_2$]$^{2+}$ Complexes: Photophysical, Spectroscopic, and Density Functional Theory Analysis

Mariana R. Camilo, Carolina R. Cardoso, Rose M. Carlos,* and A. B. P. Lever*

Photochemical and photophysical properties of the *cis*-[Ru^{II}(α-diimine)$_2$(4-APy)$_2$]$^{2+}$ complexes, where α-diimine = 1,10-phenanthroline and 4-APy = 4-aminopyridine **I**, 4,7-diphenyl-1,10-phenanthroline **II**, 2,2′-bipyridine **III**, and 4,4′-dimethyl-2,2′-bipyridine **IV**, are reported. In each case, 4-APy dissociates upon photolysis in acetonitrile. DFT analysis of the ground and excited states characterizes the electronic and geometric structure, and energy, of the lowest ^{3}MLCT state and of the ^{3}MC state. A second, nondissociative, ^{3}MC state, possibly playing a crucial role in solvolysis, is characterized.

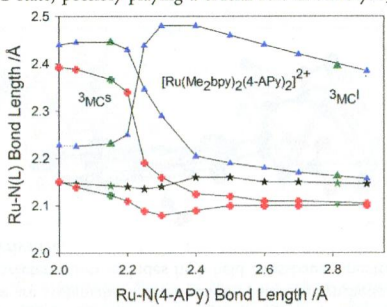

3709 dx.doi.org/10.1021/ic500026t

Good Thermoelectric Performance in Strongly Correlated System $SnCCo_3$ with Antiperovskite Structure

Shuai Lin, Peng Tong,* Bosen Wang, Jianchao Lin, Yanan Huang, and Yuping Sun*

The crystal structure and high figure of merit ZT of $SnCCo_3$ are given.

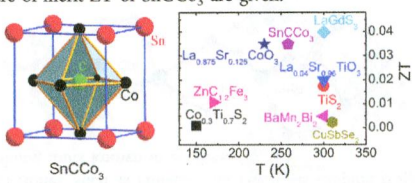

3753 dx.doi.org/10.1021/ic500083a

Construction of Larger Molecular Aluminophosphate Cages from the Cyclic Four-Ring Building Unit

Jan Chyba, Zdenek Moravec, Marek Necas, Sanjay Mathur, and Jiri Pinkas*

Six new molecular aluminophosphates of different nuclearity were synthesized by a stepwise process starting with alkane elimination from trialkylalanes and bis(trimethylsiloxy)phosphoric acid. The cyclic dimeric aluminophosphate, $[(AlMe_2\{\mu_2\text{-}O_2P(OSiMe_3)_2\})_2]$, served as a precursor in construction of larger molecular units by reactions with $OP(OH)(OSiMe_3)_2$ as a cage-extending reagent and with diketones, such as Hhfacac and Hacac, as capping reagents. The structurally characterized products contain 4=1 and S4R building units known in zeolites.

3763 dx.doi.org/10.1021/ic500086k

Iron Nitrosyl "Natural" Porphyrinates: Does the Porphyrin Matter?

Graeme R. A. Wyllie, Nathan J. Silvernail, Allen G. Oliver, Charles E. Schulz, and W. Robert Scheidt*

The synthesis and characterization of three five-coordination $\{FeNO\}_7$ porphyrin derivatives based on natural porphyrin substitution patterns show that there are systematic differences compared to synthetic porphyrin derivatives with more symmetric substitution patterns. Characterization includes high-field Mössbauer spectroscopy and a crystal structure of the protoporphyrin IX dimethyl ester derivative.

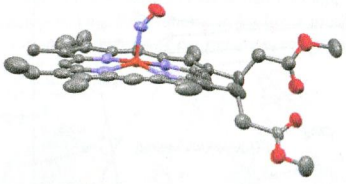

3769 dx.doi.org/10.1021/ic500106a

Origin of Ferroelectricity in a Family of Polar Oxides: The Dion—Jacobson Phases

Nicole A. Benedek*

Using symmetry principles, crystal chemical methods, and first-principles calculations, we unravel the crystal chemical origin of ferroelectricity in the Dion–Jacobson phases and show that the hybrid-improper mechanism can provide a unifying explanation for the emergence of polar structures in this family of materials.

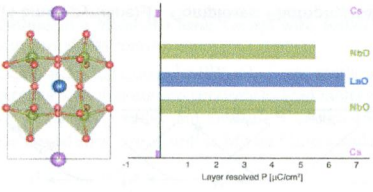

3778 S dx.doi.org/10.1021/ic500113g

Low-Coordinate Bismuth Cations

Ryan J. Schwamm, Benjamin M. Day, Martyn P. Coles,* and Christopher M. Fitchett

The synthesis of low-coordinate bismuth cations supported by the chelating diamide ligand $[Me_2Si\{NAr\}_2]^{2-}$ is described. The group 13 compounds MCl_3 (M = Al, Ga) are effective chloride abstraction agents affording mono- or dibismuth cations, depending on reaction stoichiometry. Attempted generation of the corresponding $[BR_4]^-$ salts was prevented by transfer of the R-group to Bi, affording neutral $Bi(Me_2Si\{NAr\}_2)R$ (R = Ph, Et).

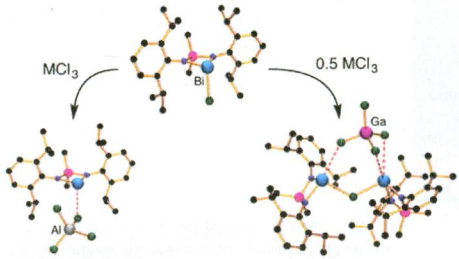

3788 S dx.doi.org/10.1021/ic500142z

Fluorescent Rhenium-Naphthalimide Conjugates as Cellular Imaging Agents

Emily E. Langdon-Jones, Nadine O. Symonds, Sara E. Yates, Anthony J. Hayes, David Lloyd, Rebecca Williams, Simon J. Coles, Peter N. Horton, and Simon J.A. Pope*

A 4-amino-substituted 1,8-naphthalimide fluorophore has been functionalized with a dipicolyl amine unit allowing a series of fluorescent Re(I) complexes to be synthesized. The ligands and complexes were investigated for their potential as cellular imaging agents for human osteoarthritic cells and protistan fish parasite *Spironucleus vortens* using confocal fluorescence microscopy. The precise structure of the ligand controls uptake and intracellular distributions.

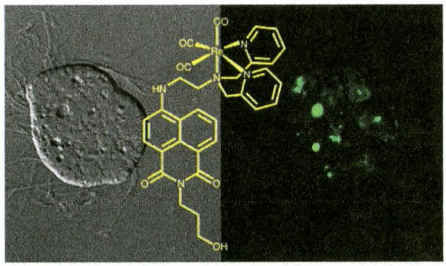

3798 dx.doi.org/10.1021/ic500145r

Synthesis, Structures, and Optical Properties of Ruthenium(II) Complexes of the Tris(1-pyrazolyl)methane Ligand

Benjamin J. Coe,* Madeleine Helliwell, Martyn K. Peers, James Raftery, Daniela Rusanova, Koen Clays, Griet Depotter, and Bruce S. Brunschwig

New Ru^{II} complexes of the tris(1-pyrazolyl)methane ligand display intense, broad visible absorptions due to metal-to-ligand charge-transfer transitions. Hyper-Rayleigh scattering, Stark spectroscopy, and density functional theory are used to probe and rationalize their optical and electronic properties. These chromophores show relatively large first hyperpolarizabilities β with substantial two-dimensional character, and comparisons are made with related *cis*-$\{Ru^{II}(NH_3)_4\}^{2+}$ complexes.

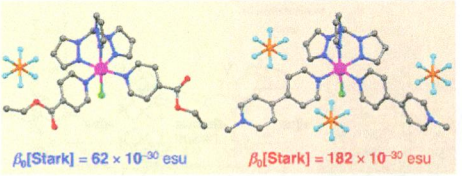

3812 dx.doi.org/10.1021/ic500156e

Spin Exchange and Magnetic Dipole–Dipole Interactions Leading to the Magnetic Superstructures of MAs_2O_6 (M = Mn, Co, Ni)

Hyun-Joo Koo* and Myung-Hwan Whangbo*

$CoAs_2O_6$ and $NiAs_2O_6$ adopt the (0, 0, 1/2) magnetic superstructure because the M–O···O–M spin exchange J_1 dominates over the other spin exchanges. For the incommensurate superstructure (0.055, 0.389, 0.136) found for $MnAs_2O_6$, the spin exchanges are not a deciding factor, but the magnetic dipole–dipole interactions are.

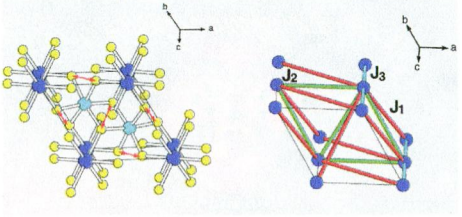

3818 dx.doi.org/10.1021/ic500161e

The Redox Chemistry of $[Co_6C(CO)_{15}]^{2-}$: A Synthetic Route to New Co-Carbide Carbonyl Clusters

Iacopo Ciabatti, Cristina Femoni, Mohammad Hayatifar, Maria Carmela Iapalucci, Giuliano Longoni, Calogero Pinzino, Matilde Valeria Solmi, and Stefano Zacchini*

The redox chemistry of $[Co_6C(CO)_{15}]^{2-}$ was studied in detail, and this species appears to be a very versatile starting material for the preparation of several Co-carbide carbonyl clusters.

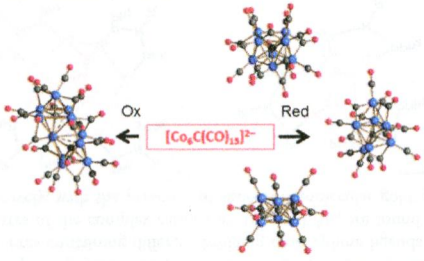

3832 S dx.doi.org/10.1021/ic5001683

Tribenzylamine C–H Activation and Intermolecular Hydrogen Transfer Promoted by WCl_6

Marco Bortoluzzi, Fabio Marchetti,* Guido Pampaloni, and Stefano Zacchini

The 1:1 molar reaction of WCl_6 with tribenzylamine selectively affords equimolar amounts of the relevant iminium and ammonium $[WCl_6]^-$ salts via amine-to-tungsten electron transfer and provides a rare example of well-understood interaction of a tertiary amine with a high-valent metal halide.

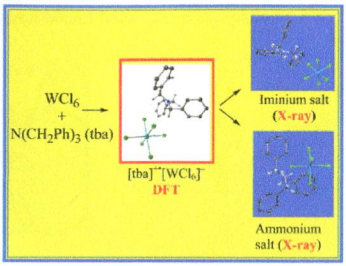

3839 S dx.doi.org/10.1021/ic5001717

The New NH-Acid $HN(C_6F_5)(C(CF_3)_3)$ and Its Crystalline and Volatile Alkaline and Earth Alkaline Metal Salts

Julius F. Kögel, Lars H. Finger, Nicolas Frank, and Jörg Sundermeyer*

The new NH-acidic amine $HN(C_6F_5)(C(CF_3)_3)$ was used for the preparation of Li, Na, K, Cs, Mg, Ca, and Ba complexes with characteristic M–F–C secondary ligand interactions in the single-crystalline state. We observed an unexpectedly high volatility and a remarkable thermal stability for the Li and Mg salts.

3847 S dx.doi.org/10.1021/ic5001842

$KSbB_2O_6$ and $BaSb_2B_4O_{12}$: Novel Boroantimonates with 3D Anionic Architectures Composed of 1D Chains of SbO_6 Octahedra and B_2O_5 Groups

Chao Huang, Jian-Han Zhang, Chun-Li Hu, Xiang Xu, Fang Kong, and Jiang-Gao Mao*

Two new boroantimonates, namely, $KSbB_2O_6$ and $BaSb_2B_4O_{12}$, have been successfully synthesized through high-temperature solid state reactions. Their structures feature two types of novel 3D anionic frameworks composed of 1D chains of corner-sharing SbO_6 octahedra that are interconnected by B_2O_5 groups.

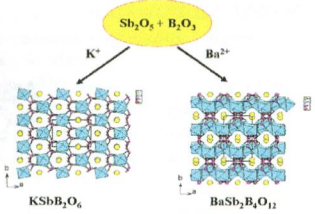

3854 S dx.doi.org/10.1021/ic500215d

Synthesis, Characterization, and Luminescence Studies of Discrete Polynuclear Gold(I) Sulfido and Selenido Complexes with Intramolecular Aurophilic Contacts

Eddie Chung-Chin Cheng, Wing-Yin Lo, Terence Kwok-Ming Lee, Nianyong Zhu, and Vivian Wing-Wah Yam*

The synthesis, characterization, and photophysical and photochemical properties of a family of high-nuclearity luminescent gold(I) sulfido and selenido complexes containing different bridging diphosphine ligands with nuclearities of 10 and 6 are reported. The X-ray crystal structures of the complex cations of Au_{10} and Au_6 are found to be propeller-like structures and distorted cubane structures, respectively, with the presence of short intramolecular gold···gold distances.

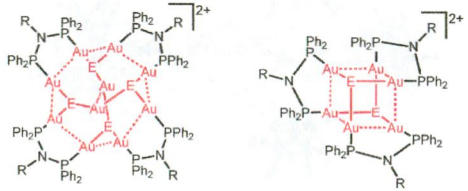

3864 S dx.doi.org/10.1021/ic500240j

Short-Bite PNP Ligand-Supported Rare Tetranuclear $[Cu_4I_4]$ Clusters: Structural and Photoluminescence Studies

Susmita Naik, Joel T. Mague, and Maravanji S. Balakrishna*

The iodo cluster $[(CuI)_4\{C_6H_5N\{P(OC_6H_4C_3H_5\text{-}o)_2\}_2\}_2]$, with a Cu–Cu distance of 2.568 Å, shows cluster-centered photoluminescence in the solid state.

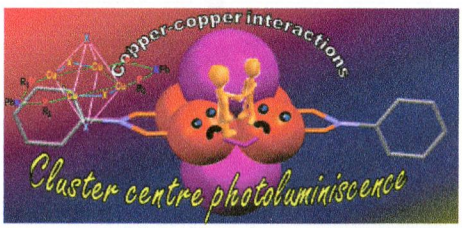

3874 S dx.doi.org/10.1021/ic500271f

Chiral $(LH)_2L_2Cu_3$ Trinuclear Paramagnetic Nodes in Octacyanidometalate-Bridged Helical Chains

Olaf Stefańczyk, Michał Rams, Anna M. Majcher, Corine Mathonière, and Barbara Sieklucka*

Trinuclear chiral $(LH)_2L_2Cu_3$ assemblies containing achiral 1,3-diamino-2-propanol are linked by octacyanidometalate(IV) forming 1D right- and left-handed helical chains arranged in an alternate manner. Magnetic studies reveal antiferromagnetic interactions inside trinuclear Cu(II) nodes leading to an $S_T = 1/2$ ground state for both assemblies.

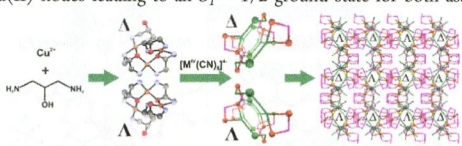

3880 S

dx.doi.org/10.1021/ic500332s

Azidophosphenium Cations: Versatile Reagents in Inorganic Synthesis

Christian Hering, Maximilian Hertrich, Axel Schulz,* and Alexander Villinger

The reactivity of azidophosphenium species with respect to their intrinsic potential to react in Staudinger reactions has been investigated. We report on the synthesis and characterization of differently substituted aminophosphenium species, in which azidophosphenium ions are incorporated. This study suggests that azidophosphenium salts can be used effectively in inorganic synthesis.

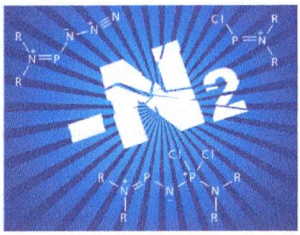

3893 S

dx.doi.org/10.1021/ic500334e

De Novo Structure-Based Design of Ion-Pair Triple-Stranded Helicates

Chuandong Jia, Benjamin P. Hay,* and Radu Custelcean*

We present a computer-aided approach toward the design of ion-pair ML_3A helicates (M = metal cation; A = anion; L = ditopic ligand), which consists of defining the C_3-symmetrical metal and anion helicate vertices based on existing structural data and identifying appropriate linkers to connect the two vertices. This approach led to identification of synthetically accessible ditopic ligands that are structurally encoded to form charge-neutral ion-pair helicates with $FeSO_4$ or $LnPO_4$.

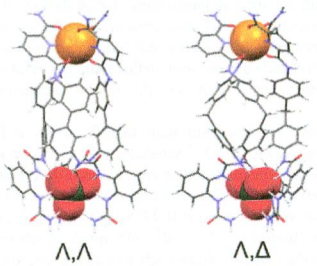

3899 S

dx.doi.org/10.1021/ic5003989

Synthesis and Characterization of Aluminum-α-diimine Complexes over Multiple Redox States

Bren E. Cole, Jeffrey P. Wolbach, William G. Dougherty Jr., Nicholas A. Piro, W. Scott Kassel, and Christopher R. Graves*

Aluminum-α-diimine complexes have been prepared in both the −1 and −2 oxidation states of the ligand. The complexes have been characterized structurally, spectroscopically, and using quantum chemistry. The electrochemical analysis shows that the Al-α-diimine complexes exhibit multiple features corresponding to the diimine^{2-}/diimine^{-} and diimine^{-}/diimine^{0} redox couples. The redox chemistry of the complexes can be coupled to reactivity chemistry at the aluminum ion.

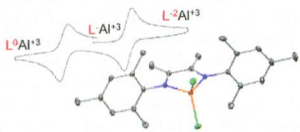

3907 Ⓢ dx.doi.org/10.1021/ic5005209

Effects of Heteroatoms on Electronic States of Divanadium-Substituted γ-Keggin-type Polyoxometalates
Kazuhiro Uehara, Takuya Miyachi, Takahito Nakajima, and Noritaka Mizuno*

The effects of substituents and heteroatoms on the electronic states of the divanadium-substituted γ-Keggin-type polyoxometalates (POMs) were investigated, using a combination of nuclear magnetic resonance spectroscopy and density functional theory calculations. Analysis of the structural and electronic characteristics of a series of POMs revealed a linear correlation between both $^{51}V\{H\}$ and ^{183}W chemical shifts and the reciprocal values of the energy gaps (ΔE^{-1}) between the LUMO+X and the XO_4-predominant orbital and demonstrated an inverse electronegativity dependence.

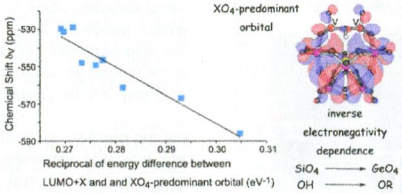

Additions and Corrections

3919 dx.doi.org/10.1021/ic5005227

Correction to Synthesis, Molecular and Electronic Structure of $U^V(O)[N(SiMe_3)_2]_3$
Skye Fortier, Jessie L. Brown, Nikolas Kaltsoyannis,* Guang Wu, and Trevor W. Hayton*

Ⓢ Supporting Information available via online article